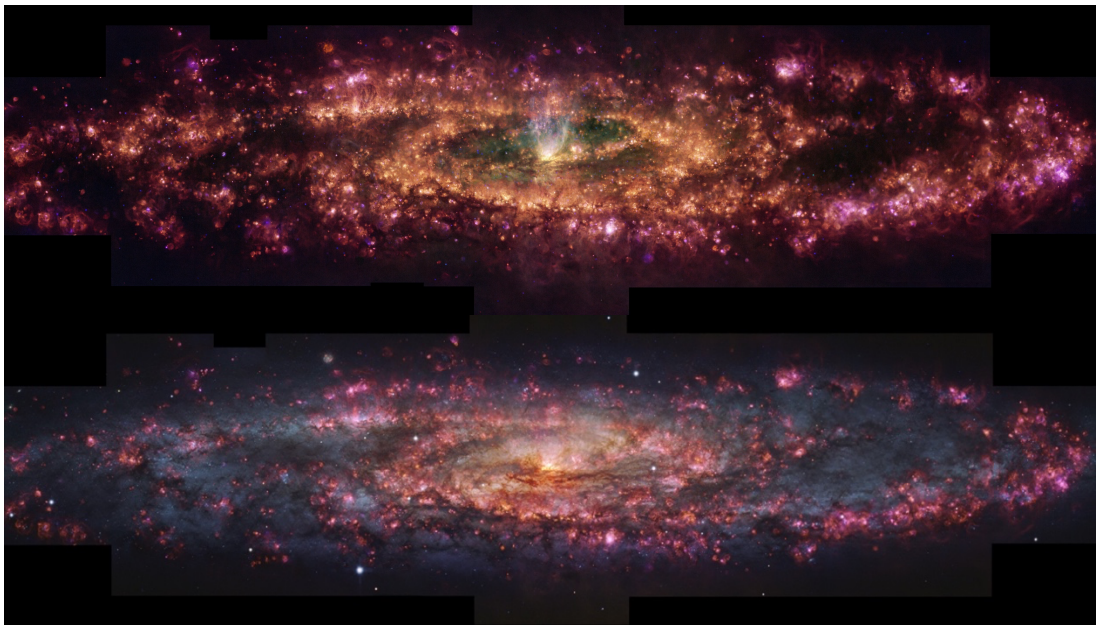
ESO Science Archive Facility - Phase 3 Data Release Description
ESO programme Unveiling the fountain: the MUSE view on the Sculptor, Data Release DR1
provided by Enrico Congiu, submitted on 2025-07-12, published on 2025-07-18

[1]The MUSE view of the Sculptor galaxy



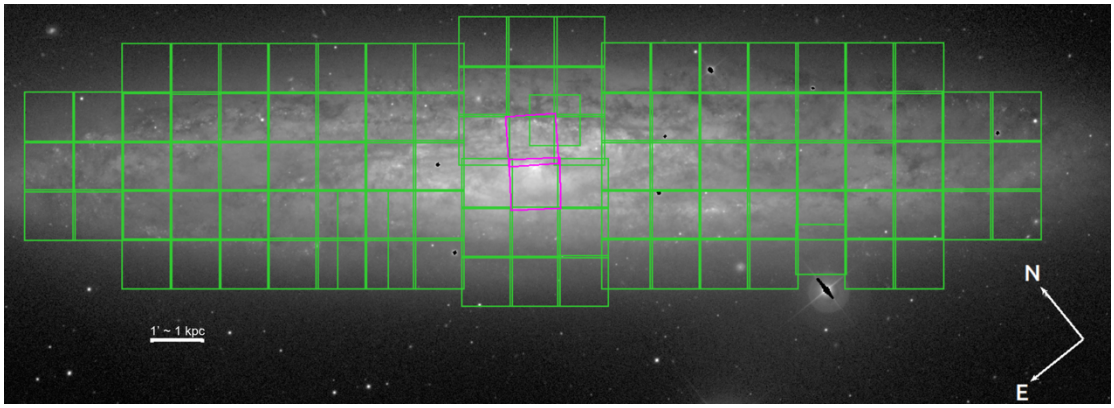
Abstract

We present the first data release of *The MUSE View of the Sculptor* programme, a survey conducted with the MUSE integral field spectrograph at the VLT to map the entire star-forming disk of the Sculptor galaxy, NGC 253. The final data product is a single mosaic combining observations from two ESO normal programmes (108.2289, PI: Congiu; and 0102.B-0078, PI: Zschaechner), covering an area of 20 × 5 arcmin^2 with 103 individual pointings. All observations were obtained with MUSE in its Wide Field Mode (WFM) and extended wavelength configuration. The majority of the dataset (101 pointings, from programme 108.2289) was acquired without adaptive optics (AO) and with relatively shallow exposure times (~850 s). The two central pointings (from programme 0102.B-0078), covering the nucleus of the galaxy, were observed with AO and longer exposures (~2000 s). The average point spread function (PSF) full width at half maximum (FWHM) across the mosaic is ~0.80″ at 5000 Å, estimated by fitting a sample of planetary nebulae (PNe) with a Moffat profile. With this release, we provide the fully mosaicked datacube of the galaxy, along with maps of derived data products including emission-line fluxes, gas and stellar kinematics, moment maps, and additional quantities extracted using the PHANGS Data Analysis Pipeline (DAP). All data are astrometrically aligned and absolute flux calibrated where applicable.

[1] Press release image credit: ESO/E. Congiu et al. – see here

Overview of Observations

Figure 1: *WFI R-band image overlaid with the positions of the observed pointings. The green squares indicate the positions observed in programme 108.A-2289, while the magenta squares correspond to programme 0102.B-0078. The white scale bar represents 1 arcmin (~1 kpc).*



This data release is based on data acquired as part of the "the MUSE view on the Sculptor" programme (108.2289), supplemented by data available on the archive and acquired as part of programme 0102.B-0078. A detailed presentation of the data, the reduction and analysis process can be found in Congiu et al. (2025). The 108.2289 data were acquired by MUSE in WFM-NOAO-E configuration, while the 0102.B-0078 observations were acquired in WFM-AO-E. Figure 1 show the position of each individual pointing on top of an R-band Wide Field Imager (WFI) image.

Release Content

The mosaic is centered at RA = 00:47:33.36 and Dec = –25:17:14.8, covering an area of approximately 20 × 5 arcmin^2. Table 1 summarizes basic properties of the observed OBs, including the observation date, programme ID, average airmass and DIMM seeing during the observation, exposure time per pointing, and the FWHM estimated from fits to PNe within the field of view. Each OB typically contains observations of two pointings, with the exception of the two OBs from programme 0102.B-0078 and the final OB of 108.2289, which each include a single pointing.

This data release includes both the main datacube and a suite of ancillary derived products. We provide:

- The fully mosaicked datacubes at native spatial and spectral resolution, including variance and data quality extensions
- Whitelight, **g**-, **r**-, and **i**-band images extracted from the datacube
- A range of data products derived from spectral fitting using the PHANGS-DAP (Data Analysis Pipeline)

The output of the DAP (Data Analysis Pipeline) are organized in a multi extension fits file, and are given in Tables 2 and 3.

Emission line velocity dispersions are not deconvolved from the instrumental resolution. In the FITS file, we include the expected instrumental dispersion in the at the wavelength of the considered line as described in Bacon et al. 2017.

The total data volume of this release is ~350 GB. The datacube is the largest file (~340 GB), followed by the file containing the output of the DAP (~10 GB).

Table 1: *Summary of the observations.*

OB Name	Date	Program	Airmass	Seeing	Exptime	FWHM1	FWHM2
WFM-NGC-253-NW	2019-07-29	0102.B-0078(A)	1.06	0.80	1960.0	0.70	-[a]
WFM-NGC-253-SE	2018-11-07	0102.B-0078(A)	1.07	0.85	1960.0	0.72	-[a]
WFM-NGC253_Pri01	2021-11-27	108.2289.001	1.21	0.58	844.8	0.74	0.79
WFM-NGC253_Pri02	2021-11-30	108.2289.001	1.09	0.55	844.8	0.85	0.82
WFM-NGC253_Pri03	2021-12-07	108.2289.001	1.32	0.84	844.8	0.99	1.15
WFM-NGC253_Pri04	2021-12-28	108.2289.001	1.23	0.51	844.8	0.68	0.76
WFM-NGC253_Pri05	2021-12-29	108.2289.001	1.22	0.77	844.8	0.91	0.78
WFM-NGC253_Pri06	2022-06-29	108.2289.001	1.17	0.49	844.8	0.69	0.84
WFM-NGC253_Pri07	2022-07-02	108.2289.001	1.33	0.57	844.8	-[b]	0.50
WFM-NGC253_Pri08	2022-07-02	108.2289.001	1.13	0.53	844.8	0.63	0.64
WFM-NGC253_Pri09	2022-07-04	108.2289.001	1.04	0.83	844.8	0.84	0.72
WFM-NGC253_Pri10	2022-08-20	108.2289.001	1.04	0.55	844.8	0.71	0.62
WFM-NGC253_Pri11	2022-08-27	108.2289.001	1.11	0.42	844.8	0.57	0.60
WFM-NGC253_Pri12	2022-08-27	108.2289.001	1.02	0.85	844.8	0.70	0.86
WFM-NGC253_Pri13	2022-08-27	108.2289.001	1.11	0.83	844.8	0.62	0.69
WFM-NGC253_Pri14	2022-09-03	108.2289.001	1.04	0.82	844.8	0.76	0.81
WFM-NGC253_Pri15	2022-09-03	108.2289.001	1.03	0.65	844.8	0.70	0.60
WFM-NGC253_Pri16	2022-09-05	108.2289.001	1.08	0.73	844.8	0.64	0.99
WFM-NGC253_Pri17	2022-09-05	108.2289.001	1.24	0.93	844.8	0.69	0.89
WFM-NGC253_Pri18	2022-09-06	108.2289.001	1.22	0.74	844.8	0.67	1.50
WFM-NGC253_Pri18	2023-01-16	108.2289.001	1.53	0.52	844.8	0.72	0.74
WFM-NGC253_Pri19	2022-09-19	108.2289.001	1.03	1.04	844.8	1.32	1.15
WFM-NGC253_Pri20	2022-09-19	108.2289.001	1.12	1.03	844.8	1.01	0.90
WFM-NGC253_Pri21	2022-09-19	108.2289.001	1.30	1.00	844.8	0.95	-[b]
WFM-NGC253_Pri22	2022-09-20	108.2289.001	1.03	1.07	844.8	1.25	1.04
WFM-NGC253_Pri23	2022-09-20	108.2289.001	1.02	1.63	844.8	1.31	1.61
WFM-NGC253_Pri24	2022-09-21	108.2289.001	1.10	0.60	844.8	0.67	0.85
WFM-NGC253_Pri25	2022-09-22	108.2289.001	1.17	0.78	844.8	1.01	0.96
WFM-NGC253_Pri26	2022-09-22	108.2289.001	1.09	0.74	844.8	-[b]	0.96
WFM-NGC253_Pri27	2022-09-23	108.2289.001	1.33	0.98	844.8	0.84	1.13
WFM-NGC253_Pri28	2022-09-23	108.2289.001	1.13	0.85	844.8	0.90	1.16
WFM-NGC253_Pri29	2022-09-23	108.2289.001	1.03	0.94	844.8	1.11	0.88
WFM-NGC253_Pri30	2022-09-23	108.2289.001	1.03	0.95	844.8	0.78	0.73
WFM-NGC253_Pri31	2022-09-24	108.2289.001	1.23	1.24	844.8	1.18	0.58
WFM-NGC253_Pri32	2022-09-24	108.2289.001	1.07	0.71	844.8	0.63	0.66
WFM-NGC253_Pri33	2022-09-24	108.2289.001	1.21	0.60	844.8	0.56	0.64
WFM-NGC253_Pri34	2022-09-25	108.2289.001	1.08	1.03	844.8	1.13	0.82
WFM-NGC253_Pri35	2022-09-25	108.2289.001	1.03	0.58	844.8	0.51	0.65
WFM-NGC253_Pri36	2022-09-26	108.2289.001	1.16	0.82	844.8	0.88	0.84
WFM-NGC253_Pri37	2022-09-26	108.2289.001	1.04	0.98	844.8	0.98	0.79
WFM-NGC253_Pri38	2022-09-26	108.2289.001	1.05	0.70	844.8	0.59	0.76
WFM-NGC253_Pri39	2022-09-29	108.2289.001	1.03	0.73	844.8	0.64	0.65
WFM-NGC253_Pri40	2022-09-30	108.2289.001	1.13	0.68	844.8	0.71	0.72
WFM-NGC253_Pri41	2022-09-30	108.2289.001	1.03	0.80	844.8	0.61	0.87
WFM-NGC253_Pri42	2022-09-30	108.2289.001	1.02	1.03	844.8	0.89	0.83
WFM-NGC253_Pri43	2022-10-28	108.2289.001	1.05	0.70	844.8	0.68	0.70
WFM-NGC253_Pri44	2022-08-26	108.2289.001	1.04	0.47	844.8	0.49	0.58
WFM-NGC253_Pri45	2022-01-04	108.2289.001	1.34	0.74	844.8	0.84	0.71
WFM-NGC253_Pri46	2022-10-28	108.2289.001	1.24	0.57	844.8	0.69	0.76
WFM-NGC253_Pri47	2022-10-30	108.2289.001	1.03	0.57	844.8	0.81	0.74
WFM-NGC253_Pri48	2022-10-30	108.2289.001	1.04	0.41	844.8	0.58	0.60
WFM-NGC253_Pri49	2022-10-30	108.2289.001	1.14	0.52	844.8	0.66	0.63
WFM-NGC253_Pri50	2023-01-15	108.2289.001	1.52	0.52	844.8	0.72	0.74
WFM-NGC253_Pri51	2023-05-30	108.2289.001	1.39	0.79	844.8	0.84	-[a]

Notes. We report the name of the OB, the date of observation, the program ID, the average airmass of the observations, the average seeing estimated from the Paranal DIMM, the exposure time, and the average full width at half maximum (FWHM) of the point spread function (PSF) for each pointing observed in the OB as derived from the PNe in Sec. 3.2. All OBs except for WFM-NGC-253-NW, WFM-NGC-253-SE, and WFM-NGC253_Pri51, include two separate pointings (see Sec 2). The exposure time refers to the single pointing. [(a)] These OBs include only a single pointing. [(b)] No PNe in the field of view of these pointings.

Table 2: *list of data products and corresponding extension name in the FITS file.*

Extension name	Description
	Binning
FLUX	white-light image
SNR	continuum S/N ratio for individual spaxels
SNRBIN	continuum S/N for each Voronoi bin
BIN_ID	unique ID for each Voronoi bin, unbinned spectra have bin IDs of −1
	Stellar kinematics
HN#_STARS = higher order Gauss-Hermite velocity moment, if available (e.g. H3_STARS, H4_STARS)	
V_STARS	stellar velocity [km s^{-1}], after subtracting the systemic velocity
FORM_ERR_V_STARS	formal velocity error [km s^{-1}]
SIGMA_STARS	stellar velocity dispersion [km s^{-1}]
FORM_ERR_SIGMA_STARS	formal sigma error [km s^{-1}]
ERR_SIGMA_STARS	MCMC-calculated error for sigma (if available) [km s^{-1}]
HN#_STARS	higher order moments of the stellar LOSVD (when available)
FORM_ERR_HN#_STARS	formal errors in the high-order moments
ERR_HN#_STARS	MCMC errors for higher order moments (not yet available)
	Stellar populations
STELLAR_MASS_DENSITY	stellar mass surface density [$M_\odot$ pc^{-2}]
STELLAR_MASS_DENSITY_ERR	error in the above [$M_\odot$ pc^{-2}]
AGE_MW	log(Age/yr), where the Age is mass-weighted
AGE_MW_ERR	error in the above quantity
Z_MW	mass-weighted [Z/H]
Z_MW_ERR	error in the above quantity
AGE_LW	log(Age/yr), where the Age is luminosity-weighted (V-band)
AGE_LW_ERR	error in the above
Z_LW	luminosity-weighted (V-band) [Z/H]
Z_LW_ERR	error in the above quantity
EBV_STARS	$E(B-V)$ of the stellar component [mag]
	Emission lines
*emline = emission line string id listed in Table B.3	
BIN_ID_LINES	unique bin for emission lines, these are individual spaxels in the current DR2
CHI2_TOT	The χ^2 over the full fitted wavelength range.
*emline_FLUX	emission line flux [10^{-20} erg s^{-1} cm^{-2} spaxel^{-1}]
*emline_FLUX_ERR	emission line flux error [10^{-20} ergs^{-1}cm^{-2} spaxel^{-1}]
*emline_VEL	emission line velocity [km s^{-1}]
*emline_VEL_ERR	emission line velocity error [km s^{-1}]
*emline_SIGMA	emission line velocity dispersion [km s^{-1}]
*emline_SIGMA_ERR	emission line velocity dispersion error [km s^{-1}]
*emline_SIGMA_CORR	instrumental velocity dispersion at the position of the line [km s^{-1}]
*emline_MOM0	emission line moment 0 [10^{-20} erg s^{-1} cm^{-2} spaxel^{-1}]
*emline_MOM0_ERR	emission line moment 0 error [10^{-20} ergs^{-1}cm^{-2} spaxel^{-1}]
*emline_MOM1	emission moment 1 [km s^{-1}]
*emline_MOM1_ERR	emission moment 1 error [km s^{-1}]
*emline_MOM2	emission moment 2 [km s^{-1}]
*emline_MOM2_ERR	emission moment 2 error [km s^{-1}]

Notes. Each extension is a two-dimensional map on the same WCS as the mosaic datacube. We list the extension names, and a brief description of the map associated with that extension. All lines maps produced are corrected for the Milky Way foreground contribution. Moment-zero maps are not.

Table 3: *list of emission lines included in the FITS file.*

Line name	Wavelength (air) [Å]	String ID	Ionisation potential [eV]	Fixed ratio
		Hydrogen Balmer lines		
Hβ	4861.35	HB4861	13.60	no
Hα	6562.79	HA6562	13.60	no
		Low ionisation lines		
[N II]λ5197	5197.90	NI5197	—	no
[N II]λ5200	5200.26	NI5200	—	no
[N II]λ5754	5754.59	NII5754	14.53	no
[N II]λ6548	6548.05	NII6548	14.53	0.34 [N II]λ6584
[N II]λ6584	6583.45	NII6583	14.53	no
[S II]λ6717	6716.44	SII6716	10.36	no
[S II]λ6731	6730.82	SII6730	10.36	no
		High-ionisation lines		
He IIλ4686	4685.70	HEII4865	24.58	no
[O III]λ4959	4958.91	OIII4958	35.12	0.35 [O III]λ5007
[O III]λ5007	5006.84	OIII5006	35.12	no
He Iλ5876	5875.61	HEI5875	—	no
[S III]λ6312	6312.06	SIII6312	23.34	no

Notes. Wavelengths are taken from the National Institute of Standards and Technology (NIST; https://physics.nist.gov/PhysRefData/ASD/lines_form.html), and are Ritz wavelengths in air except for the H Balmer lines, in which case we use the 'observed ' wavelength in air as reported in NIST. The DAP string name is used to identify the correct extension in the MAPS files or in the moment maps. Ionisation potentials are taken from Draine (2011). The [O I] lines at 6300 and 6363 Å are not included in this list because they are heavily contaminated by sky emission.

Release Notes

The data have been reduced using pymusepipe (Emsellem et al. 2022), a Python wrapper around the MUSE data reduction pipeline (Weilbacher et al. 2020). Our reduction procedure closely follows that of Emsellem et al. (2022), with some modifications related to sky subtraction and alignment due to the proximity of the galaxy, as well as improvements to the existing software. For details specific to the data reduction of NGC 253, see Congiu et al. (2025).

We first applied the standard recipes of the MUSE data reduction pipeline v2.9.0 to remove instrumental signatures, including bias subtraction, flat-field and illumination corrections, wavelength and line spread function (LSF) calibrations, and initial geometric and astrometric alignment. The wavelength solution is provided in the barycentric reference frame, and all wavelengths are air wavelengths.

To refine the astrometry, align individual exposures, and improve flux calibration, we used an R-band image of NGC 253. This image was produced using the PHANGS imaging pipeline (A. Razza et al., in prep.) to reduce archival data obtained with the WFI instrument, available from the ESO archive. The astrometry of this reference image— and therefore of the final datacube and all derived products— is tied to Gaia DR2. The alignment has been performed using spacepylot (https://github.com/ejwatkins-astro/spacepylot).

Data Reduction and Calibration

Data Cubes - Photometric calibration and sky subtraction

Offset sky exposures are used to produce a sky spectrum. We then used the reference R-band images to simultaneously constrain the sky subtraction and the global flux normalisation (per exposure). Assuming that the R-band reference image has zero background and the correct absolute flux normalisation, and that the flux in the MUSE reconstructed image represents a linear function of the true flux (involving a normalisation constant plus a background), we can write:

$$\begin{aligned} \mathrm{Flux}_{\mathrm{Rband}}(x,y) &= a \times \mathrm{MUSE}_1^R(x,y) \\ &= a \times \left(\mathrm{MUSE}_{\mathrm{raw}}^R(x,y) + \mathrm{Sky} - \mathrm{Sky}_1\right) + b \end{aligned}$$

where Sky is a constant representing the true sky background for that specific exposure, Sky_1 is another constant representing the actual value removed during the initial sky subtraction process, and a and b are constants representing a linear regression representation of the $\mathrm{Flux}_{\mathrm{Rband}}$ versus the MUSE reconstructed image. A perfect sky subtraction and normalisation would lead to a=1 and b=0. We then use the fitted a value as a normalisation correction, and b to fix the sky contribution by applying $Sky = \alpha \times Sky_1$ where $\alpha = 1 - b/(a \cdot Sky_1)$. Hence, knowing a and b as well as Sky_1, the value of the sky continuum integrated within the reference image filter, we derive a correction for the sky normalisation that yields a linear regression where b=0.

It is important to note that the sky renormalisation only acts within the R-band filter, assuming that the reference image is background free. Since the reference MUSE sky exposure may result in a reference sky spectrum that is not necessarily an exact representation of the actual sky on the MUSE science exposure, this could lead to a colour variation, hence to an over- or under-subtraction of the sky which depends on wavelength.

Data Cubes - Image reconstruction

We follow an approach that minimizes the need for resampling by using a table-based representation of the data (PixelTables), as implemented in the MUSE data reduction scripts. Just before starting the mosaicing procedure, the PixelTables are used to reconstruct the datacubes for each individual exposure, ensuring that all cubes are projected onto the same astrometric grid. This enables

a seamless combination of the exposures into a mosaic, without requiring additional interpolations.

For this release, no PSF homogenization procedure has been applied, so the PSF varies across the mosaic depending on the atmospheric conditions at the time of each exposure. The average PSF for each pointing (after the combination of its four exposures) was estimated by fitting a sample of planetary nebulae (PNe) and is reported in Table 1.

Data Products - Stellar continuum fitting

Prior to the fitting process, the MUSE data cube is corrected for foreground Galactic extinction, using the O'Donnell et al. (1994) extinction law and the values from Schlafly et al. (2011; see sample $E(B-V)$ table above). The data are then Voronoi binned to a target S/N of 35. This S/N level is used to determine both the stellar kinematics and the stellar population properties. The stellar kinematics are derived using pPXF2 (Cappellari & Emsellem 2004, Cappellari 2017), following the same procedure as implemented by Bittner et al. (2019) in gist (https://abittner.gitlab.io/thegistpipeline/) . Note that the data cubes provided in the data release are "as observed"and thus do not include any correction for extinction (which is only applied during the analysis process). Briefly, to fit the stellar continuum we use E-MILES simple stellar population models (Vazdekis et al. 2016), generated with a Chabrier et al. (2003) initial mass function, BaSTI isochrones (Pietrinferni et al. 2004), eight ages (0.15 -14 Gyr, logarithmically spaced in steps of 0.22 dex) and four metallicities ([Z/H] = [-1.5, -0.35, 0.06, 0.4]), for a total of 32 templates. We fit the wavelength range 4600 - 7000 Å in order to avoid strong sky residuals in the redder part of the MUSE wavelength range. The regions around the expected positions of ionised gas emission lines and sky lines are masked. To derive the stellar kinematics, we make use of additive Legendre polynomials (12th order, in the spectral direction), and no multiplicative polynomials.

Data Products - Emission line fitting

The MUSE data cube is corrected for foreground Galactic extinction as for the stellar continuum fitting process. The fits are performed on individual spaxels, and the stellar kinematics is fixed to that of the Voronoi bin to which the spaxel was associated during the stellar kinematics fitting step. Emission lines are fitted by performing an independent call to pPXF, where emission lines are treated as additional Gaussian templates, and the stellar continuum is fitted simultaneously. Some of the code we use to interface with pPXF in this fitting stage was adapted directly from the MaNGA data analysis pipeline (Westfall et al. 2019), and makes use of the analytical Fourier transform implemented in version > 6 of pPXF (Cappellari et al. 2017).

The kinematic parameters of the emission lines (velocity and velocity dispersion) are tied in three groups, as follows:

1. Hydrogen Balmer lines: Hα, Hβ;
2. Low-ionisation lines: [O I]$\lambda\lambda$6300,64, [N I]$\lambda\lambda$5197,5200, [N II]$\lambda\lambda$6548,84, [N II]λ5754, [S II]$\lambda\lambda$6717,31;
3. High-ionisation lines: [He I]λ5875, [O III]$\lambda\lambda$4959,5007, [S III]λ6312.

We tie the intrinsic (astrophysical) velocity dispersion within each kinematic group, prior to convolution with the instrumental LSF. During the emission lines fit, pPXF is run with 8th order multiplicative Legendre polynomials, but no additive polynomials.

Data Products – Emission lines moment maps

This release includes, moment 0, 1, and 2 maps for all the lines fitted by the DAP. They have been computed using a reference velocity of 235.36 km/s and a window of ±400 km/s using continuum subtracted cubes produced. Please, note the following:

- The window used for the computation of the moments is relatively large. In case of lines closed together and broad, there might be some cross-contamination between them.
- Since cross-contamination is impossible to avoid for the [SII] doublet, we created a moment 0 map using a larger window that includes both lines.
- Moment 0 maps should be reliable in general, and several of them have already been used

in Congiu et al. (2025).

- Moment 1 and 2 should be handled with care, since they are usually much more sensitive to the choice of the window and the masking of the spectrum. When computing them, we mask all spaxels with negative values.

Data Quality

Astrometry

The astrometry of the reference image was calibrated using a large sample of stars located outside the galaxy. To assess the accuracy of this calibration within the galaxy itself, we identified a smaller sample of stars inside the galaxy and measured their offsets relative to positions from the *Gaia* DR3 catalog. This comparison revealed negligible astrometric offsets: 0.02 ± 0.60 arcsec in right ascension and 0.03±0.46 arcsec in declination. We registered the MUSE astrometry using the *spacepylot* software package. While this method is generally reliable, small residual shifts or localized rotational misalignments may still be present in some regions of the image.

Flux Calibration

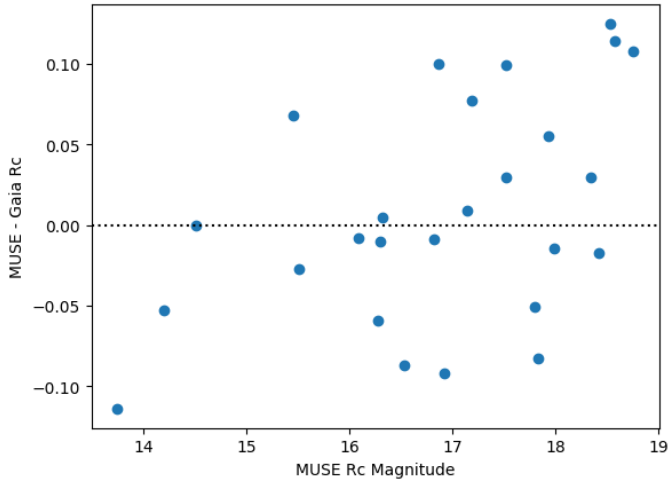


Figure 2: *Comparison between R-Cousins magnitudes derived from MUSE data and Gaia photometry — We compared the R-Cousins magnitudes derived from MUSE datacube images with Gaia photometry for a sample of stars with Gaia G-band magnitudes between 14 and 19, located within our MUSE mosaic. The MUSE magnitudes were obtained via aperture photometry using a 3″ aperture, with local background subtraction performed in a thin annulus surrounding the aperture. Gaia magnitudes were converted to R-band magnitudes using the color–magnitude relations provided in Table 5.9 of the Gaia DR3 documentation. The root-mean-square error (RMSE) between the Gaia-derived and MUSE magnitudes is approximately 0.07 mag, corresponding to a photometric uncertainty of about 6%.*

Known issues

AO Mode

While the vast majority of the pointing has been acquired with WFM-NOAO, the two central pointings, recovered from the archive, have been observed in WFM-AO. In this case, some Raman scattered lines can be part of the spectrum. The two brightest are: O2 6484.39, N2 6827.17. Please consider masking these regions when using the spectra. It also means that the wavelength range encompassing the laser emission has been masked for these two pointings and is missing from the datacube. In addition, these regions should also be ignored in the maps associated with the [NII]5754 and HeI5875 lines, since they fall inside this gap.

Line contamination from sky emission

NGC 253 recession velocity is of the order of 240 km/s with a rotation curve of ~ +-180 kms. This means that for the approaching side of the galaxy, at the MUSE spectral resolution of ~50 km/s, several emission lines overlap with (bright) sky emission lines. The most affected lines are Ha, [OI]6300, [OI]6363, [OI]5577.

To improve the quality of the sky subtraction, the pipeline uses the sky offset to identify the sky emission lines and then the science offset to rescale the flux of these lines. However, it is not able to differentiate between the overlapping sky and object lines, which results in artifacts (mostly over-subtraction). We managed to mitigate this effect on the most important line, Ha, by directly subtracting the Ha flux measured in the sky offset without rescaling. This is possible because the sky Ha emission is relatively faint and stable in time. Since the [OI] lines are highly variable, this approach is not possible and for now, we decided to not perform any action on them. Some PCA analysis in the future might help with retrieving the flux for some of the [OI] lines too. Since this effect mostly the approaching side of the galaxy, we still fit the [OI] lines in the DAP, but be aware that only the parts corresponding to the receding side of the galaxy are reliable.

Image alignment

We identified a few issues associated with the geometric and astrometric solutions provided via predefined MUSE calibrations. About 20% of all exposures exhibit a global small but still significant rotation between 0.1 and 0.3 degrees with respect to the R-band images, with no apparent correlation with RA, DEC or time when the target was observed. This residual rotation is corrected for.

Imperfect sky subtraction: effect on stellar extinction

Overall, we conclude that we may slightly under-estimate the noise level by 10 to 30% when using the derived variances (and ignoring the covariance terms), and that the `bias' due to improper sky continuum subtraction is present and negligible for most of the spectra, but can be significant for about 10 to 20% of them, especially towards the blue end of the MUSE wavelength range. By construction, there are no offsets in the broad-band color reconstructed images of individual pointings. We confirm that we observe no systematic differences between adjacent pointings using such broad-band filters, a good a posteriori check of our implementation. This is, however, not necessarily true for colors. The spectral dependence of the median bias suggests that the shape of the sky continuum spectrum used for the sky background subtraction process may sometimes depart from the true one. Fixing such an issue would require a spectrally-dependent correction of the reference sky spectrum itself. This may be addressed by using photometric reference points (e.g., HST imaging) in several bands (as opposed to the
single Rc band used here), but it is beyond the scope of the present release.

Bad DAP fit in the center

Due to the large amount of dust extinction in the galaxy (see Congiu et al. 2025), the DAP struggles to successfully fit the central regions, particularly in the blue part of the spectrum. This results in artifacts in the central area of all maps associated with emission lines below ~5200 Å. We tested several strategies to mitigate the issue—such as increasing or decreasing the degree of the polynomial used during the fit, or restricting the fitted wavelength range—but none fully resolved the problem. As a result, these artifacts are still present in the released version of the data. However, they affect only a small portion of the mosaic.

Previous Releases

N/A

Data Format

Files Types

The main data product released is the mosaiced datacube of NGC 253. Datacubes for the individual pointings are not included in this release. The mosaic is provided as a multi-extension FITS file, which includes four extensions:

NGC0253.fits
(PRODCATG = SCIENCE.CUBE.IFS)

- **Primary**: Contains the main header.
- **DATA** (EXTNAME=DATA) **:** The science data cube.
- **STAT** (EXTNAME=STAT) **:** The variance cube.
- **DQ** (EXTNAME=DQ) **:** The data quality cube.

This main datacube is accompanied by the following ancillary products:

- **NGC0253_PHANGS_whitelight.fits**
  (PRODCATG=ANCILLARY.IMAGE.WHITELIGHT)
  A white-light image obtained by averaging the datacube across all available wavelengths.

- **NGC0253_PHANGS_{filter}.fits**
  (PRODCATG=ANCILLARY.IMAGE)
  Images extracted using three SDSS broadband filters, where {filter} = SDSS_r, SDSS_g, or SDSS_i. **Note**: The SDSS g- and i-band filters are only partially covered by the MUSE spectral range. Where necessary, the AO gap in the MUSE wavelength coverage is linearly interpolated.

- **NGC0253_PHANGS_MAPS.fits**
  (PRODCATG=ANCILLARY.IMAGE)
  A multi-extension FITS file containing all the quantities derived from fitting the datacube with pPXF, as well as the moment maps. Tables 2 and 3 list and describe the included extensions.

Catalogue Columns

N/A

Acknowledgements

According to the Data Access Policy for ESO data held in the ESO Science Archive Facility, all users are required to acknowledge the source of the data with appropriate citation in their publications.

Since processed data downloaded from the ESO Archive are assigned Digital Object Identifiers (DOIs), the following statement must be included in all publications making use of them:

- *Based on data obtained from the ESO Science Archive Facility with DOI: https://doi.org/10.18727/archive/100*

Publications making use of data which have been assigned an archive request number (of the form XXXXXX) must include the following statement in a footnote or in the acknowledgement:

- *Based on data obtained from the ESO Science Archive Facility under request number <request_number>.*

The dataset and data reduction associated with this data release is described in detail in Congiu et al. (2025, accepted). Please cite this paper when making use of this dataset. The paper is available at the following link: https://doi.org/10.1051/0004-6361/202554144.

The link is also available on the PHANGS web site: Publications

Science data products from the ESO archive may be distributed by third parties, and disseminated via other services, according to the terms of the Creative Commons Attribution 4.0 International license. Credit to the ESO provenance of the data must be acknowledged, and the file headers preserved.

References:

Bacon, R., et al. 2017, A&A, 608, A1;
Bittner, A., et al. 2019, A&A, 628, A117;
Cappellari, M. & Emsellem, E. 2004, PASP, 116, 138;
Chabrier, G. 2003, PASP, 115, 763;
Congiu E., et al. 2025, A&A, in press https://doi.org/10.1051/0004-6361/202554144;
Emsellem E., et al. 2022, A&A, 659, A191;
O'Donnell J. E. 1994, ApJ, 422, 158;
Pietrinferni, A., et al. 2004, ApJ, 612, 168;
Schlafly, E. F. & Finkbeiner, D. P. 2011, ApJ, 737, 103;
Vazdekis, A., et al. 2016, MNRAS, 463, 3409;
Weilbacher P. M., Palsa, R., Streicher, O., et al. 2020, A&A, 641, A28;
Westfall, K. B., et al. 2019, AJ, 158, 231.